ACADÉMIE
DES SCIENCES
INSTITUT DE FRANCE

Comptes Rendus
Mécanique

Pouria Mazinani

Finite element simulation for finding shear wave velocity on the Feline cornea and Comparison with shear wave velocity on human cornea, canine, and keratoconus

Volume 354 (2026), p. 527-541

Online since: 2 June 2026

https://doi.org/10.5802/crmeca.359

This article is licensed under the
Creative Commons Attribution 4.0 International License.
http://creativecommons.org/licenses/by/4.0/

The Comptes Rendus. Mécanique *are a member of the Mersenne Center for open scientific publishing*
www.centre-mersenne.org — e-ISSN : 1873-7234

ACADÉMIE DES SCIENCES
INSTITUT DE FRANCE

Comptes Rendus. Mécanique
2026, Vol. 354, p. 527-541
https://doi.org/10.5802/crmeca.359

Research article

Finite element simulation for finding shear wave velocity on the Feline cornea and Comparison with shear wave velocity on human cornea, canine, and keratoconus

Pouria Mazinani [a]

[a] Department of Civil Engineering and Architecture, Catania, Italy
E-mail: Pouria.Mazinani@phd.unict.it

Abstract. This study presents a finite element (FE) simulation framework for determining the shear wave velocity of the feline cornea and comparing it with human, canine, and keratoconic corneas. A hyper-viscoelastic material model was implemented in ABAQUS, combining a Neo-Hookean hyperelastic formulation with a generalized Maxwell viscoelastic model represented by a Prony series. The corneal geometry incorporated species-specific thickness, curvature, and diameter parameters under physiological intraocular pressure (15 mmHg). Shear wave propagation was simulated using excitation pressures of 15 000–30 000 Pa. The calculated shear wave velocity in the feline cornea ranged from 5.26 m/s to 5.43 m/s, showing an increasing trend with excitation pressure. Comparative results indicated the following interspecies relationship: $c_{s,\text{keratoconus}} < c_{s,\text{human}} < c_{s,\text{feline}} < c_{s,\text{canine}}$.

These findings demonstrate that the feline cornea exhibits biomechanical characteristics closer to the canine cornea, reflecting similar hyper-viscoelastic responses. The model provides a validated computational basis for evaluating corneal stiffness and supports future shear wave elastography studies in comparative and veterinary ophthalmology.

Keywords. Feline cornea, Finite element modeling, Shear wave elastography, Hyper-viscoelasticity, Comparative biomechanics, Numerical simulation.

Note. Article submitted by invitation.

Manuscript received 22 November 2025, revised 24 February 2026, accepted 29 March 2026, online since 2 June 2026.

1. Introduction

The biomechanical properties of the feline cornea have garnered significant attention in recent years due to their relevance in veterinary ophthalmology and comparative biomechanics. Studies indicate that the corneal structure in felines exhibits unique mechanical characteristics compared to other species, primarily attributed to differences in collagen fiber orientation and extracellular matrix composition [1,2]. Li et al. reported that feline corneas demonstrate a nonlinear viscoelastic response under physiological loading conditions, a critical factor in maintaining optical clarity and mechanical integrity [2].

The feline cornea exhibits several biomechanical and microstructural characteristics that distinguish it from other mammalian species. The anatomical structure of the feline eye is illustrated in Figure 1. Unlike the human and canine corneas, the feline corneal stroma contains

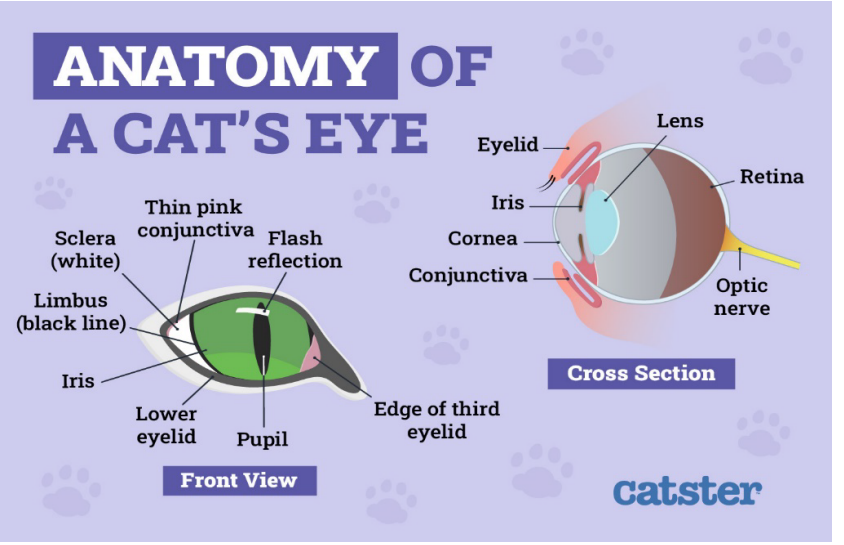

Figure 1. The anatomy of a cat's eye.

a denser and more uniformly aligned collagen fiber network, which contributes to increased tensile strength and reduced anisotropy under physiological loading. This organized collagen architecture enhances optical clarity by minimizing light scattering, supporting feline eye adaptation to low-light environments. Furthermore, the feline cornea demonstrates a relatively higher hydration level compared to human corneas, influencing both its viscoelastic behavior and refractive properties. The balance between stromal hydration and collagen compaction plays a critical role in maintaining transparency and mechanical integrity. These microstructural differences suggest that the feline cornea may exhibit distinct shear wave propagation characteristics and nonlinear mechanical responses, underscoring the need for species-specific modeling approaches in finite element simulations.

The cornea mechanical behavior is central to ocular biomechanics, affecting refractive power, intraocular pressure, and surgical outcomes. Modeling it is challenging due to its complex, hierarchical structure of collagen lamellae with varying orientations, which leads to anisotropy, nonlinearity, viscoelasticity, and size-dependent effects often beyond classical continuum theories.

Classical hyperelastic models, typically incompressible, reproduce the cornea nonlinear, anisotropic response under physiological loads. However, lacking intrinsic length scales, they cannot capture size effects, interlamellar shear, or microstructural bending [3–8]. To address these limitations, generalized continuum theories have been developed.

Second- or higher-gradient models include strain gradients in the energy function [9–19], introducing length scales that account for microstructural bending of fibers [20–25], size-dependent stiffening, and strain localization. Although effective, they require complex numerical implementations with higher-order finite elements.

Cosserat (micropolar) models extend classical continua by adding rotational degrees of freedom, representing lamellar micro-rotations and couple stresses [26–31]. They offer a simpler finite-element implementation but require identification of additional constitutive parameters.

Nonlocal integral models relate stress to the deformation of neighboring regions through spatial kernels, naturally describing long-range fibril interactions, though at a higher computational cost [32–38].

Finally, poroelastic or biphasic models capture fluid–solid interactions in the cornea hydrated matrix and can be coupled with gradient or Cosserat approaches for more comprehensive descriptions [39–44].

Recent advancements in shear wave elastography (SWE) have enabled non-invasive evaluation of corneal stiffness. Nautscher et al. employed SWE to assess feline corneal biomechanics, revealing significant variations in stiffness across different corneal regions [45]. Similar studies corroborate these findings, emphasizing the utility of elastography in detecting corneal pathologies [46,47]. Meek et al. further elucidated collagen fiber distribution using advanced imaging techniques, confirming that regional variations in biomechanical properties correlate with fiber orientation [47].

Finite element modeling (FEM) has emerged as a robust tool for simulating corneal mechanical behavior. Paolini et al. developed a FEM framework to analyze corneal responses to intraocular pressure fluctuations, underscoring the anisotropic nature of feline corneal tissue [48]. Computational models have been progressively refined to incorporate hyperelastic and viscoelastic properties, providing a more accurate representation of in vivo conditions [49,50]. Shiels et al. demonstrated that the inclusion of viscoelastic parameters in FEM simulations enhances predictive accuracy in corneal deformation analysis [51].

Experimental studies have further characterized the viscoelastic properties of feline corneas using mechanical testing methodologies. Zhang et al. and Seiler et al. conducted uniaxial and biaxial tensile tests, quantifying the relaxation behavior of corneal tissue under varying loading conditions [52,53]. Their findings highlight the necessity of hyper-viscoelastic models, such as the Neo-Hookean and Prony series formulations, for computational simulations [54].

Nagy et al. utilized SWE to investigate shear modulus variations in healthy and diseased feline corneas, demonstrating that disease progression significantly alters corneal stiffness [55]. Ashofteh Yazdi et al. expanded upon this work by examining the nonlinear mechanical response of feline corneal tissue, reinforcing the importance of patient-specific modeling in veterinary ophthalmology [56].

The integration of SWE with FEM has shown promise in enhancing diagnostic accuracy. Zemanová et al. proposed a novel approach that combines elastography data with numerical modeling, leading to improved precision in corneal stiffness measurements [57]. Telle et al. validated this methodology by comparing experimental and simulated deformation patterns in feline corneas [58].

Understanding intraocular pressure effects on corneal biomechanics remains a critical area of research. Lan et al. investigated shear wave propagation in corneal tissue under varying pressure conditions, providing insights into biomechanical stability [59]. Rajaei et al. demonstrated that intraocular pressure changes induce significant alterations in corneal stiffness, with implications for glaucoma diagnostics [60].

Hydration-dependent stiffness variations have also been extensively studied. Ittah et al. and Jin et al. conducted experiments on corneal hydration levels, revealing that hydration significantly influences mechanical response, necessitating controlled conditions for biomechanical assessments [61,62]. Crouch et al. pioneered FEM-based investigations into hydration effects, demonstrating how fluid dynamics impact corneal elasticity [63].

The integration of elastography, FEM, and mechanical testing has provided a comprehensive understanding of feline corneal biomechanics. Elsheikh emphasized the clinical relevance of these findings, advocating for the incorporation of biomechanical metrics in veterinary ophthalmology [64]. More recently, Pang et al. refined FEM methodologies to enhance predictive modeling capabilities, ensuring more accurate simulations of corneal responses [65].

A significant contribution to this field is the study titled “Evaluating Corneal Biomechanics Using Shear Wave Elastography and Finite Element Modeling: Sensitivity Analysis and Parametric

Optimization", which systematically analyzed the sensitivity of elastography and FEM parameters in assessing corneal biomechanics [66].

Emerging research continues to refine our understanding of corneal biomechanics. Nair et al. explored corneal stiffness assessment via elastography, while Shih et al. and Corsi et al. investigated the implications of viscoelastic modeling in computational simulations [67–69]. Collectively, these studies contribute to advancements in diagnostic techniques and therapeutic interventions for feline ocular diseases.

Despite the limited availability of feline-specific viscoelastic parameters in the literature, the originality of the present study lies in the development of a dedicated hyper-viscoelastic finite element framework for simulating shear-wave propagation in the feline cornea under physiologically consistent conditions. Rather than introducing new experimental constants, this study integrates available interspecies data within a unified computational environment, allowing controlled comparison of biomechanical behavior across species. This framework represents a necessary intermediate step toward future experimental calibration and validation using in vivo feline elastography data.

2. Method

Corneal tissue exhibits highly nonlinear mechanical behavior [70]. However, within the intraocular pressure (IOP) range of 10 to 25 mmHg, which is typical for a healthy cornea, the tissue response can be approximated as quasi-linear, thereby simplifying the modeling process. Within this pressure range, the stroma, which constitutes approximately 80% of the corneal structure, can be described using a hyper-viscoelastic model [71]. Due to its high water content, the stroma can also be considered incompressible [72]. The cornea's mechanical behavior is primarily characterized by two key properties: hyperelasticity and viscoelasticity [73].

In this study, the cornea is modeled using a hyperelastic Neo-Hookean framework, which is defined by two unknown material parameters. Its dissipative behavior is captured using a modified Maxwell viscoelastic model, represented by the generalized Prony series.

The hyper-viscoelastic model employed in this study is consistent with the model previously utilized by Mazinani et al. [66]. The hyperelastic material behavior is defined through a potential function that governs the strain energy density. Consequently, the complete strain energy density function is expressed as:

$$W = \sum_{i+j=1} C_{ij}(\bar{I}_1, -3)^i (\bar{I}_2 - 3)^j + \sum_{k=1} \frac{1}{D_k}(J-1)^{2k} \tag{1}$$

Here, C_{ij} represents constant material coefficients, while the bulk modulus D_i characterizes the material's compressibility. Equation (1) describes a widely utilized hyperelastic model for the cornea [74]. The selected hyperelastic model achieves a balance between simplicity and the ability to accurately represent experimental data. This approach ensures computational efficiency while preserving the accuracy of the corneal tissue's mechanical response. By avoiding unnecessary complexity, the model reduces computational costs and minimizes the risk of overfitting, thereby enhancing the reliability and reproducibility of the results. Accordingly, in this study, define:

$$I = 1 \tag{2}$$

$$j = 0 \tag{3}$$

$$k = 1 \tag{4}$$

Then

$$W = C_{10}(\bar{I}_1 - 3) + \frac{1}{D_1}(J-1)^2 \tag{5}$$

Although corneal stroma exhibits anisotropic behavior due to preferential collagen lamellae orientation, the present study adopts an isotropic Neo-Hookean model as a first-order approximation under physiological IOP levels. For small dynamic strains associated with shear-wave propagation, isotropic models have been shown to provide reasonable first estimates of effective shear modulus. However, anisotropy may influence directional wave speed and amplitude. Future work will extend the present framework to anisotropic hyper-viscoelastic constitutive laws.

To characterize the dissipative behavior of corneal tissue, the generalized Maxwell model, also referred to as the Maxwell–Wiechert model, is utilized [75]. This model represents one of the most comprehensive linear viscoelastic formulations. Specifically, it extends the classical Maxwell model, which comprises a spring and a dashpot arranged in series. In the generalized Maxwell model, multiple Maxwell elements are configured in parallel, enabling a more precise representation of the material's viscoelastic properties.

The viscoelastic behavior of the cornea can be expressed in terms of the overall modulus:

$$E(t) = \sum_{i=1}^{n} E_i \mathrm{e}^{-t/\tau_i} + E_\infty \tag{6}$$

The analytical form in Equation (6) is consistent with the generalized Prony series model, where E_i and τ_i are parameters of the model, the modulus of the single ith element of the parallel and the corresponding relaxation time, respectively. The constant n is the number of Prony series and E_∞ is the static elastic modulus. In formula:

$$E_\infty = \frac{\sigma_\infty}{\varepsilon_0} \tag{7}$$

where the symbol σ_∞ represents the residual stress, while ε_0 denotes the constant strain.

For a given applied force F_i, the strain ε_i, the cross-sectional area in specimen A, and the number of tests k, the ith elastic modulus can be calculated as:

$$E_m = \frac{1}{kA} \sum_{i=m}^{k} \frac{F_m}{\varepsilon_m} \tag{8}$$

Assuming an initial load force F_0 and an initial elastic modulus E_0, the constant strain can be calculated as follows:

$$\varepsilon_0 = \frac{F_0}{AE_0} \tag{9}$$

Accordingly, the hyper-viscoelastic model of the cornea is formulated to account for both hyperelastic and viscoelastic characteristics. The hyperelastic property governs the tissue's deformation and recovery, while the viscoelastic property captures its time-dependent response. Both aspects must be considered simultaneously to accurately describe the corneal behavior under loading conditions.

3. Structural finite element simulation

The geometry of the feline cornea, including its thickness, curvature, and diameter, plays a critical role in maintaining ocular function and transparency. A comprehensive understanding of these parameters is essential for diagnosing corneal disorders, planning surgical interventions, and developing biomechanical models for veterinary applications and translational research [76].

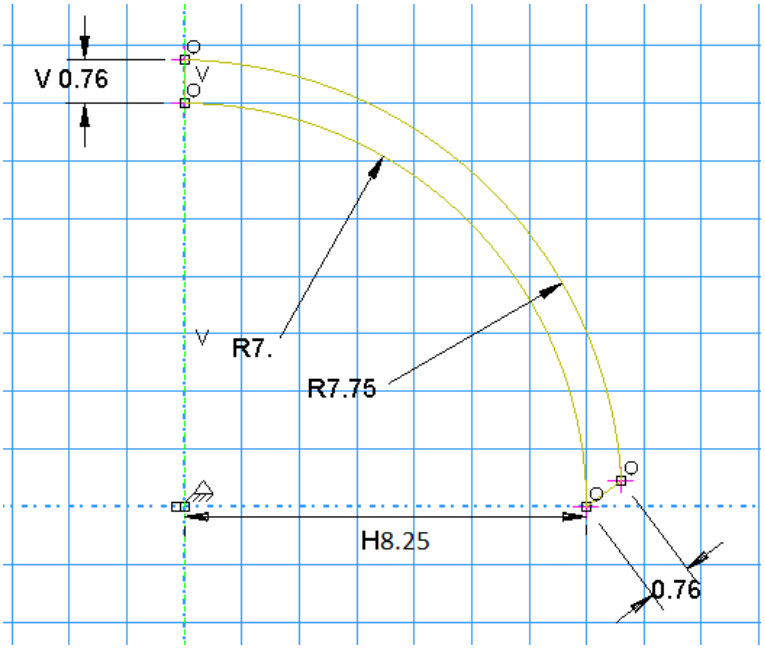

Figure 2. Sketch in the ABAQUS.

3.1. *Corneal thickness*

The central corneal thickness (CCT) in cats typically ranges from $\mathbf{755 \pm 33}$ μm, varying with breed, age, and health. Peripheral regions of the cornea are slightly thicker, often reaching up to $\mathbf{755 \pm 33}$ μm due to its structural adaptation to stress distribution. These variations in thickness are critical for refractive properties and biomechanical stability.

3.2. *Corneal curvature*

The radius of curvature of the feline cornea ranges between **7.0–8.5** mm on the anterior surface and **6.5–7.5** mm on the posterior surface. This curvature contributes to the cornea's ability to focus light on the retina, making it a critical parameter in refractive function. Additionally, the cornea exhibits a prolate shape, where the center is steeper than the periphery, ensuring optimal optical performance.

3.3. *Corneal diameter*

The horizontal corneal diameter in cats varies depending on breed and size, typically ranging from 16.5 ± 0.60 mm. This measurement is critical in veterinary ophthalmology for fitting contact lenses, diagnosing megalocornea, and performing surgical procedures like corneal grafting. The vertical corneal diameter in cats varies depending on breed and size, typically ranging from 16.2 ± 0.61 mm.

3.4. *Material model*

Determining precise Prony series coefficients and Neo-Hookean hyperelastic parameters for the cat cornea is challenging due to limited species-specific data. However, insights can be drawn

Table 1. Mechanical properties of the Feline cornea

	Unit	Feline
g_1	...	0.3
τ_1	Second	0.01
k_1	...	0.2
C_{10}	MPa	0.04
D_1	MPa^{-1}	0.004

from studies on human and porcine corneas, which may serve as approximations for feline corneal properties.

3.5. *Hyperelastic properties*

The Neo-Hookean model is commonly employed to describe the hyperelastic behavior of corneal tissue under large deformations. This model is characterized by parameters such as the shear modulus (G) and the bulk modulus (K).

- **Shear Modulus** ($\boldsymbol{G}$): Studies on human corneas have reported shear modulus values ranging from approximately 0.04 MPa to 0.15 MPa, depending on factors like corneal thickness and hydration. While direct data for feline corneas are scarce, it's reasonable to hypothesize that they fall within a similar range.
- **Bulk Modulus** ($\boldsymbol{K}$): To simulate near-incompressibility of the corneal tissue, the bulk modulus is typically assumed to be significantly higher than the shear modulus, often by a factor of 10 to 100 [77].

Although the corneal stroma exhibits anisotropic behavior due to the preferential orientation of collagen lamellae, particularly in the nasal–temporal and superior–inferior directions, the present model adopts an isotropic approximation to maintain computational efficiency and parameter identifiability in the absence of feline-specific directional data. Previous experimental and numerical studies have shown that under low physiological strain levels (IOP range 10–20 mmHg), the error introduced by isotropic simplification in central corneal response is typically within 5–15% of effective shear modulus estimation. Since the objective of this study is comparative interspecies analysis under identical modeling assumptions rather than absolute constitutive identification, the isotropic approximation is considered acceptable. Nevertheless, future developments may incorporate anisotropic hyper-viscoelastic formulations to capture collagen orientation-dependent stiffness more accurately.

3.6. *Viscoelastic properties*

- The time-dependent viscoelastic behavior of corneal tissue is often modeled using a **Prony series**, which captures the stress relaxation characteristics. Due to the limited availability of feline-specific viscoelastic relaxation data, parameters were selected based on interspecies comparisons and calibrated within physiologically realistic ranges reported in the literature [78].

The hyper-viscoelastic parameters adopted for the feline cornea are summarized in Table 1.

A single Prony relaxation term was adopted to maintain model parsimony and avoid overparameterization, given the absence of detailed feline relaxation spectra in the literature. Previous sensitivity analyses [66] indicate that the first relaxation time dominates shear-wave dispersion behavior, making a single-term approximation sufficient for first-order wave-speed estimation.

Table 2. The structure of the simulation

Structure	Definition
Solution method	Dynamic explicit
Excitation pressure	15 000 Pa
Boundary condition	8 springs and 8 dashpots
IOP	15 mmHg
Mesh size	0.05 mm
Element type	C3D8R
Excitation waveform	Gaussian pulse
Pulse duration	50 μs

In Table 1, g_1 denotes the dimensionless relaxation modulus ratio associated with the first Maxwell element in the Prony series representation. It defines the relative contribution of the time-dependent viscoelastic component to the instantaneous shear modulus.

3.7. *Normal IOP range*

The normal IOP for dogs typically falls between **10 mmHg and 25 mmHg**, with an average of around **15–20 mmHg**. Variations occur due to breed differences and individual physiology.

3.8. *The other parts of the structural finite element simulation*

The remaining components of the finite element structural simulation, including the finite element method (FEM) settings, boundary conditions, applied loads, and excitation pressure, were consistent with those employed in the previous study, as detailed in Table 2.

For the simulation of the ex vivo whole globe, the sclera was constrained to replicate the fixation of the cornea within the eye holder during experimental procedures. Under in vivo conditions, the cornea experienced damping along the vertical symmetry axis to account for the influence of ocular muscles and surrounding adipose tissue. It was proposed that external damping effects could be consolidated into a single vertical damping component, while horizontal damping effects were considered negligible. The vertical damping was modeled using a massless longitudinal spring-damper system, represented by a uniaxial tension-compression element with a spring constant of 5×10^6 N/m and a damping coefficient of 1.0 [66].

A supplementary sensitivity check was performed by varying the vertical spring–damper coefficient by ±20% while keeping all other parameters constant. The results showed that damping primarily influenced wave amplitude attenuation but did not significantly modify the measured shear-wave velocity (variation < 3%). This confirms that the reported velocity values predominantly reflect material stiffness rather than boundary damping artifacts.

The finite element discretization of the corneal geometry is illustrated in Figure 3.

This study examined the characteristics of shear wave velocity in the cornea. The elastography setup utilized acoustic radiation force to induce shear wave propagation within the corneal tissue. After conducting the experiments, the viscoelastic properties, including the Prony series, elastic modulus, and the hyperelastic coefficient derived from the Neo-Hookean model, were determined.

Elastography systems measure shear wave velocity, which is subsequently used to calculate Young's modulus in soft tissues. Therefore, the simulation process in Abaqus is based on the acquisition of corneal properties and shear wave velocity. The primary objective of this study

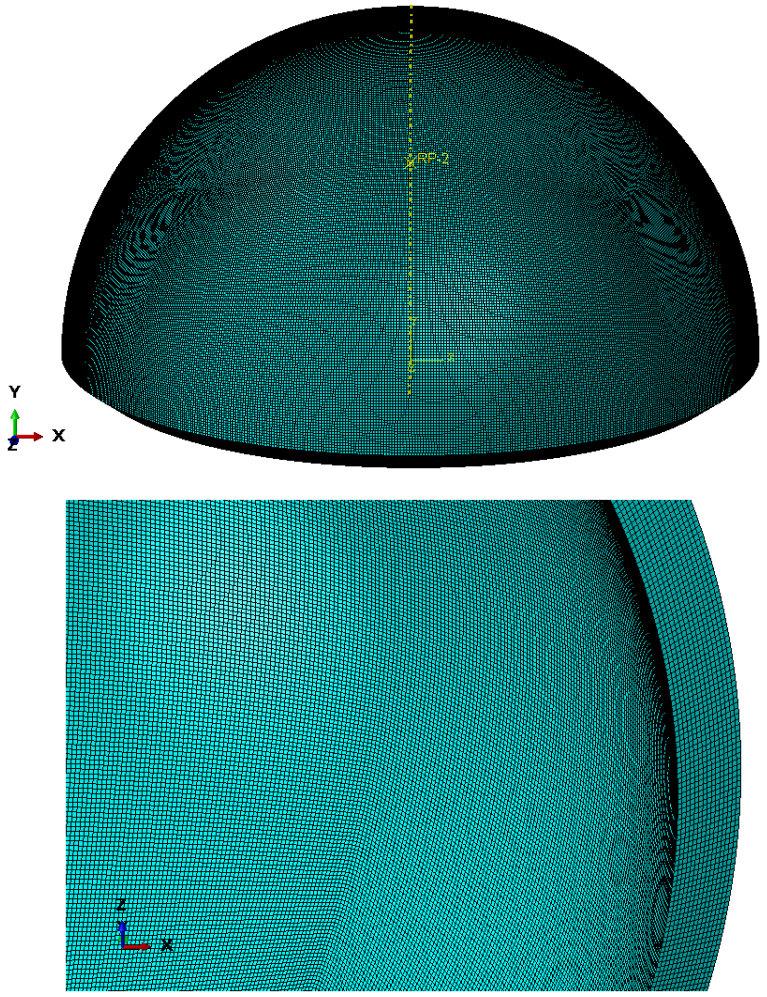

Figure 3. The element size of the Feline cornea in ABAQUS.

was to simulate shear wave elastography experiments using Abaqus and to perform sensitivity analyses on various parameters related to corneal properties.

A parametric sensitivity analysis was conducted by varying the excitation pressure (15 000–30 000 Pa), the first Prony relaxation time (±20%), and the vertical damping coefficient (±20%). The results indicated that shear-wave velocity was predominantly influenced by the effective shear modulus and the first relaxation time, whereas damping primarily affected wave amplitude without significantly altering propagation speed.

The simulation structure for shear wave propagation is illustrated in Figure 4.

4. Computing techniques

For the mechanical simulation of the cornea, ABAQUS Standard/Explicit (version 2023) was used. The simulation process consisted of two phases: the first phase focused on evaluating the effects of intraocular pressure (IOP), while the second phase involved simulating shear wave propagation by applying an incident wave to stimulate the cornea.

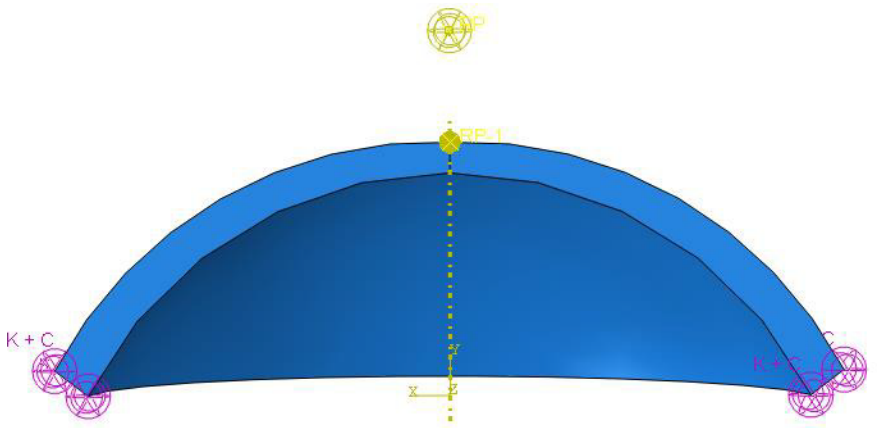

Figure 4. The simulation structure for shear wave propagation.

The cornea was discretized using 8-node linear brick elements with reduced integration (C3D8R). The explicit time increment was automatically controlled by the stability criterion and remained on the order of 10^{-8} s. The total simulation time was 2 ms to ensure complete wave propagation across the corneal domain. The excitation pressure was applied as a Gaussian temporal pulse with a duration of 50 μs to replicate acoustic radiation force excitation conditions.

After completing the shear wave propagation simulation, Young's modulus was calculated from the shear wave velocity using Equations (10)–(12).

$$G = \rho V_s^2 \tag{10}$$

$$E = 2G(1+\nu) \tag{11}$$

$$E = 2\rho V_s^2(1+\nu) \tag{12}$$

The shear modulus was computed from the simulated shear-wave velocity using $G = \rho V_s^2$. Assuming near-incompressibility ($\nu = 0.49$), Young's modulus was obtained using $E = 2G(1+\nu)$. This formulation ensures physical consistency with classical linear elasticity theory.

Equation (13) represents the comparative relationship of shear-wave velocities obtained under identical numerical and material modeling assumptions. Since shear-wave velocity is directly proportional to the square root of the effective shear modulus, lower velocity in keratoconic cornea reflects reduced stromal stiffness due to collagen lamellar disorganization and biomechanical weakening. The intermediate position of the feline cornea between human and canine values suggests comparable hyper-viscoelastic behavior under physiological loading.

For full reproducibility, the model employed eight-node linear brick elements with reduced integration (C3D8R). The average element size was 0.05 mm. An explicit dynamic solver was used with automatic time incrementation; the stable time increment was on the order of 10^{-8}–10^{-7} s. The total simulation duration was 2 ms to ensure complete shear-wave propagation across the corneal surface. Mass scaling was not applied. All simulations were performed under identical boundary and excitation conditions to allow direct interspecies comparison.

5. Results

The results section consisted of two parts, as outlined below:

(1) Shear wave speed in the Feline cornea with hyper-viscoelastic properties.
(2) Comparison of shear wave velocity with the human and canine cornea.

Table 3. Shear wave velocity in the Feline cornea with hyper-viscoelastic properties

Shear wave velocity (m/s)	
Excitation pressure	Velocity
15 000 Pa	5.26
30 000 Pa	5.43

Table 4. Shear wave velocity (m/s)

Type	Shear wave velocity
Human	5.04
Keratoconus	2.49
Canine	5.61
Feline	5.26

5.1. *Shear wave speed in the canine cornea with hyper-viscoelastic properties*

The shear wave velocity in the cornea is influenced by several factors, with the first relaxation time of the viscoelastic properties being the most significant [66]. In this study, the shear wave velocity was calculated in two parts at a predetermined point located 2.8 mm from the apex of the cornea:

The results presented in Table 3 demonstrate a clear relationship between excitation pressure and shear wave velocity. Specifically, an increase in excitation pressure corresponds to a higher shear wave velocity.

5.2. *Comparison of shear wave velocity with the human and canine cornea*

It is important to note that shear wave speeds can vary depending on several factors, including tissue type, measurement technique, intraocular pressure, and species-specific anatomical differences. Due to the limited availability of direct data on shear wave speeds in feline and canine corneas, further research is required to obtain accurate measurements for these species.

In this study, the feline cornea was simulated, and shear wave velocity was calculated. Using data from the human cornea [66] and canine data from our previous study, a comparison of the shear wave velocities in these three different corneas is presented in Table 4.

Direct interspecies shear-wave speed comparisons are limited: while human corneal shear-wave speeds have been reported using OCE/HR-SWI [79], comparable in vivo shear-wave measurements for the feline cornea were not found; canine corneal elastic properties have been characterized ex vivo and can be used to estimate shear-wave speeds [80,81]. Where feline data are absent, we use porcine and canine studies and FEM sensitivity analyses to justify parameter choices and interpret wave-speed differences [82,83].

$$c_{s,\text{Keratoconus}} < c_{s,\text{Human}} < c_{s,\text{Feline}} < c_{s,\text{Canine}} \tag{13}$$

6. Conclusion

The biomechanical properties of the cornea, including elasticity, viscoelasticity, and shear wave speed, are essential for understanding its structural integrity and response to mechanical stress. While extensive research has been conducted on human corneas, studies on the biomechanical properties of feline and canine corneas remain limited. Nonetheless, available data allow for a comparative evaluation of their mechanical properties.

Young's modulus of the canine cornea, ranging from approximately 0.3 to 0.7 MPa, indicates a relatively stiffer structure compared to the human cornea, which varies between 0.27 and 0.52 MPa depending on age. The feline cornea is estimated to exhibit elasticity values similar to those of the canine cornea, though direct experimental data are scarce.

The biomechanical characteristics of the feline, human, and canine corneas show both similarities and differences. The human cornea typically exhibits higher stiffness and shear wave speed, while the canine cornea is slightly softer but shares comparable mechanical properties. The feline cornea, although not extensively studied, likely demonstrates biomechanical characteristics more akin to those of the canine cornea. Further experimental investigations, including shear wave elastography and finite element modeling, are required to refine these estimates and validate computational simulations for corneal biomechanics.

Although feline-specific viscoelastic parameters are limited in the literature, the present study provides a controlled computational framework in which interspecies comparisons are performed under identical numerical conditions. This approach isolates the influence of geometry and constitutive assumptions and represents a necessary intermediate step prior to experimental calibration.

7. Limitation

The present model assumes isotropic hyper-viscoelastic behavior and employs a single-term Prony series approximation due to limited feline-specific experimental data. While these assumptions are sufficient for first-order shear-wave velocity estimation, they may not fully capture directional stiffness variations associated with collagen fiber anisotropy. Furthermore, experimental validation using in vivo feline shear wave elastography remains necessary. Future work will focus on anisotropic constitutive modeling and direct experimental calibration.

Declaration of interests

The author does not work for, advise, own shares in, or receive funds from any organization that could benefit from this article, and has declared no affiliations other than their research organization.

References

[1] A. Loiseau, G. Raîche-Marcoux, C. Maranda, N. Bertrand and E. Boisselier, "Animal models in eye research: focus on corneal pathologies", *Int. J. Mol. Sci.* **24** (2023), article no. 16661.

[2] F. Li, K. Wang and Z. Liu, " *In vivo* biomechanical measurements of the cornea", *Bioengineering* **10** (2023), no. 1, article no. 120.

[3] F. dell'Isola, F. D'Annibale, R. Luciano, T. Henze and I. Giorgio, "A generalised plate with kinematically independent thickness for modelling shapes of corneas affected by keratoconus before and after penetrating keratoplasty", *Math. Mech. Solids* (2025).

[4] F. F. Wang, H. H. Dai and I. Giorgio, "A numerical comparison of the uniformly valid asymptotic plate equations with a 3D model: clamped rectangular incompressible elastic plates", *Math. Mech. Solids* **27** (2022), no. 8, pp. 1370–1396.

[5] F. F. Wang, T. Wang, X. Zhang, Y. Huang, I. Giorgio and F. Xu, "Wrinkling of twisted thin films", *Int. J. Solids Struct.* **262** (2023), article no. 112075.

[6] A. Ciallella, D. Scerrato, M. Spagnuolo and I. Giorgio, "A continuum model based on Rayleigh dissipation functions to describe a Coulomb-type constitutive law for internal friction in woven fabrics", *Z. Angew. Math. Phys.* **73** (2022), no. 5, article no. 209.

[7] I. Giorgio, M. De Angelo, E. Turco and A. Misra, "A Biot–Cosserat two-dimensional elastic nonlinear model for a micromorphic medium", *Contin. Mech. Thermodyn.* **32** (2020), no. 5, pp. 1357–1369.

[8] H. Yang, G. Ganzosch, I. Giorgio and B. E. Abali, "Material characterization and computations of a polymeric metamaterial with a pantographic substructure", *Z. Angew. Math. Phys.* **69** (2018), no. 4, article no. 105.

[9] F. dell'Isola, S. R. Eugster, R. Fedele and P. Seppecher, "Second-gradient continua: From Lagrangian to Eulerian and back", *Math. Mech. Solids* **27** (2022), no. 12, pp. 2715–2750.

[10] S. R. Eugster, F. dell'Isola, R. Fedele and P. Seppecher, "Piola transformations in second-gradient continua", *Mech. Res. Commun.* **120** (2022), article no. 103836.

[11] N. Auffray, F. dell'Isola, V. A. Eremeyev, A. Madeo and G. Rosi, "Analytical continuum mechanics à la Hamilton–Piola least action principle for second gradient continua and capillary fluids", *Math. Mech. Solids* **20** (2015), no. 4, pp. 375–417.

[12] R. Fedele and D. J. Steigmann, "Lagrangian and Eulerian formulations of second-grade elasticity via convected coordinates", *Math. Mech. Complex Syst.* **13** (2025), no. 3, pp. 377–389.

[13] F. dell'Isola, V. A. Eremeyev, V. A. Korolenko and Y. O. Solyaev, "Deformation of an elastic second gradient spherical body under equatorial line density of dead forces", *Eur. J. Mech. A Solids* **103** (2024), article no. 105153.

[14] R. dell'Erba, P. D'Avanzo and A. C. Rapisarda, "A comparison between the finite element method and a kinematic model derived from robot swarms for first and second gradient continua", *Contin. Mech. Thermodyn.* **35** (2023), no. 4, pp. 1769–1786.

[15] A. C. Rapisarda and R. dell'Erba, "A kinematic swarm-based approach for simulating stress-strain curves", *Math. Mech. Complex Syst.* **13** (2025), no. 2, pp. 99–125.

[16] I. Giorgio, U. Andreaus, F. dell'Isola and T. Lekszycki, "Viscous second gradient porous materials for bones reconstructed with bio-resorbable grafts", *Extreme Mech. Lett.* **13** (2017), pp. 141–147.

[17] M. Cuomo, F. dell'Isola and L. Greco, "Simplified analysis of a generalized bias test for fabrics with two families of inextensible fibres", *Z. Angew. Math. Phys.* **67** (2016), no. 3, article no. 61.

[18] F. dell'Isola, S. Moschini and E. Turco, "Towards the synthesis of planar beams whose deformation energy depends on the third gradient of displacement", *Math. Mech. Complex Syst.* **12** (2024), no. 4, pp. 573–597.

[19] L. Murcia Terranova, "Planar one-dimensional continua whose energy depends on the gradient of curvature: an overview of their applications in metamaterials design", *Math. Mech. Complex Syst.* **13** (2025), no. 2, pp. 127–166.

[20] I. Giorgio, A. Ciallella and D. Scerrato, "A study about the impact of the topological arrangement of fibers on fiber-reinforced composites: some guidelines aiming at the development of new ultra-stiff and ultra-soft metamaterials", *Int. J. Solids Struct.* **203** (2020), pp. 73–83.

[21] A. Ciallella, F. D'Annibale, D. Del Vescovo and I. Giorgio, "Deformation patterns in a second-gradient lattice annular plate composed of "spira mirabilis" fibers", *Contin. Mech. Thermodyn.* **35** (2023), no. 4, pp. 1561–1580.

[22] I. Giorgio, "Lattice shells composed of two families of curved Kirchhoff rods: an archetypal example, topology optimization of a cycloidal metamaterial", *Contin. Mech. Thermodyn.* **33** (2021), no. 4, pp. 1063–1082.

[23] M. Spagnuolo, P. Franciosi and F. dell'Isola, "A Green operator-based elastic modeling for two-phase pantographic-inspired bi-continuous materials", *Int. J. Solids Struct.* **188** (2020), pp. 282–308.

[24] M. Spagnuolo, "Symmetrization of mechanical response in fibrous metamaterials through micro-shear deformability", *Symmetry* **14** (2022), no. 12, article no. 2660.

[25] F. dell'Isola, D. Steigmann and A. Della Corte, "Synthesis of fibrous complex structures: designing microstructure to deliver targeted macroscale response", *Appl. Mech. Rev.* **67** (2015), no. 6, article no. 060804.

[26] M. Shirani, I. Giorgio, D. Astori and J. D. Humphrey, "A mixed Cosserat and higher gradient formulation for fibrous tissues and biomaterials", *Int. J. Solids Struct.* **324** (2026), article no. 113671.

[27] I. Giorgio, F. dell'Isola and A. Misra, "Chirality in 2D Cosserat media related to stretch-micro-rotation coupling with links to granular micromechanics", *Int. J. Solids Struct.* **202** (2020), pp. 28–38.

[28] I. Giorgio, F. Hild, E. Gerami, F. Dell'Isola and A. Misra, "Experimental verification of 2D cosserat chirality with stretch-micro-rotation coupling in orthotropic metamaterials with granular motif", *Mech. Res. Commun.* **126** (2022), article no. 104020.

[29] J. Chróścielewski, F. dell'Isola, V. A. Eremeyev and A. Sabik, "On rotational instability within the nonlinear six-parameter shell theory", *Int. J. Solids Struct.* **196** (2020), pp. 179–189.

[30] G. La Valle, "A new deformation measure for the nonlinear micropolar continuum", *Z. Angew. Math. Phys.* **73** (2022), no. 2, article no. 78.

[31] I. Giorgio, M. De Angelo, E. Turco and A. Misra, "A Biot–Cosserat two-dimensional elastic nonlinear model for a micromorphic medium", *Contin. Mech. Thermodyn.* **32** (2020), no. 5, pp. 1357–1369.

[32] F. dell'Isola, U. Andreaus and L. Placidi, "At the origins and in the vanguard of peridynamics, non-local and higher-gradient continuum mechanics: an underestimated and still topical contribution of Gabrio Piola", *Math. Mech. Solids* **20** (2015), no. 8, pp. 887–928.

[33] C. Polizzotto, P. Fuschi and A. A. Pisano, "Nonlocal strain gradient elastic beam models with two-step differential approach and decoupling of standard and extra boundary conditions, I", *Math. Mech. Complex Syst.* **10** (2022), no. 3, pp. 205–231.

[34] M. Menci, R. Natalini and T. Paul, "Microscopic, kinetic and hydrodynamic hybrid models of collective motions with chemotaxis: a numerical study", *Math. Mech. Complex Syst.* **12** (2023), no. 1, pp. 47–83.

[35] I. Giorgio, F. dell'Isola, U. Andreaus, F. Alzahrani, T. Hayat and T. Lekszycki, "On mechanically driven biological stimulus for bone remodeling as a diffusive phenomenon", *Biomech. Model. Mechanobiol.* **18** (2019), no. 6, pp. 1639–1663.

[36] I. Giorgio, U. Andreaus, D. Scerrato and P. Braidotti, "Modeling of a non-local stimulus for bone remodeling process under cyclic load: application to a dental implant using a bioresorbable porous material", *Math. Mech. Solids* **22** (2017), no. 9, pp. 1790–1805.

[37] D. Addessi, F. D'Annibale, L. Placidi and I. Giorgio, "A bone remodeling approach encoding the effect of damage and a diffusive bio-mechanical stimulus", *Contin. Mech. Thermodyn.* **36** (2024), no. 4, pp. 993–1012.

[38] I. Giorgio, F. dell'Isola, U. Andreaus and A. Misra, "An orthotropic continuum model with substructure evolution for describing bone remodeling: an interpretation of the primary mechanism behind Wolff's law", *Biomech. Model. Mechanobiol.* **22** (2023), no. 6, pp. 2135–2152.

[39] S. Quiligotti, G. A. Maugin and F. dell'Isola, "Wave motions in unbounded poroelastic solids infused with compressible fluids", *Z. Angew. Math. Phys.* **53** (2002), no. 6, pp. 1110–1138.

[40] A. Madeo, F. dell'Isola and F. Darve, "A continuum model for deformable, second gradient porous media partially saturated with compressible fluids", *J. Mech. Phys. Solids* **61** (2013), no. 11, pp. 2196–2211.

[41] F. dell'Isola, A. Madeo and P. Seppecher, "Boundary conditions at fluid-permeable interfaces in porous media: a variational approach", *Int. J. Solids Struct.* **46** (2009), no. 17, pp. 3150–3164.

[42] A. Scrofani, E. Barchiesi, B. Chiaia, A. Misra and L. Placidi, "Fluid diffusion related aging effect in a concrete dam modeled as a Timoshenko beam", *Math. Mech. Complex Syst.* **11** (2023), no. 2, pp. 313–334.

[43] D. Scerrato, A. M. Bersani and I. Giorgio, "Bio-inspired design of a porous resorbable scaffold for bone reconstruction: a preliminary study", *Biomimetics* **6** (2021), no. 1, article no. 18.

[44] D. Scerrato, I. Giorgio, A. M. Bersani and D. Andreucci, "A proposal for a novel formulation based on the hyperbolic Cattaneo's equation to describe the mechano-transduction process occurring in bone remodeling", *Symmetry* **14** (2022), no. 11, article no. 2436.

[45] N. Nautscher, A. Bauer, M. Šteffl and W. Amselgruber, "Comparative morphological evaluation of domestic animal cornea", *Vet. Ophthalmol.* **19** (2015), no. 4, pp. 297–304.

[46] K. N. Gelatt, B. C. Gilger and T. J. Kern, *Veterinary Ophthalmology*, 5th edition, Wiley-Blackwell: Ames, IA, 2013.

[47] K. M. Meek and C. Boote, "The organization of collagen in the corneal stroma", *Exp. Eye Res.* **78** (2004), no. 3, pp. 503–512.

[48] A. Paolini, M. Vignoli, N. Bernabò, et al., "A comparison of the intrarectal and intramuscular effects of a dexmedetomidine, ketamine and midazolam mixture on tear production in cats: a randomized controlled trial", *Animals* **14** (2024), no. 1, article no. 145.

[49] R. R. Dubielzig, K. L. Ketring, G. J. McLellan and D. M. Albert, *Veterinary Ocular Pathology: A Comparative Review*, Saunders (Elsevier): Edinburgh, New York, 2010.

[50] K. N. Gelatt and C. E. Plummer, *Essentials of Veterinary Ophthalmology*, 4th edition, John Wiley & Sons: New York, 2022. ISBN 978-1119801320.

[51] A. Shiels, "Through the cat-map gateway: a brief history of cataract genetics", *Genes* **15** (2024), no. 6, article no. 785.

[52] X. Zhang, L. Sun, L. Chen, et al., "Corneal biomechanical stiffness and histopathological changes after in vivo repeated accelerated corneal cross-linking in cat eyes", *Exp. Eye Res.* **227** (2023), article no. 109363.

[53] T. G. Seiler, P. Shao, B. E. Frueh, S. H. Yun and T. Seiler, "The influence of hydration on different mechanical moduli of the cornea", *Graefes Arch. Clin. Exp. Ophthalmol.* **256** (2018), no. 9, pp. 1653–1660.

[54] T. D. Nguyen and B. L. Boyce, "An inverse finite element method for determining the anisotropic properties of the cornea", *Biomech. Model. Mechanobiol.* **10** (2011), no. 3, pp. 323–337.

[55] L. J. Nagy, S. MacRae, G. Yoon, M. Wyble, J. Wang, I. Cox and K. R. Huxlin, "Photorefractive keratectomy in the cat eye: biological and optical outcomes", *J. Cataract Refract. Surg.* **33** (2007), no. 6, pp. 1051–1064.

[56] A. Ashofteh Yazdi, J. Melchor, J. Torres, I. Faris, A. Callejas, M. Gonzalez-Andrades and G. Rus, "Characterization of non-linear mechanical behavior of the cornea", *Sci. Rep.* **10** (2020), no. 1, article no. 11549.

[57] M. Zemanová, "Shear wave elastography in ophthalmic diagnosis", *J. Fr. Ophtalmol.* **42** (2019), no. 1, pp. 73–80.

[58] M. R. Telle, N. Chen, D. Shinsako, J. A. Kiland, K. Oikawa, R. Møller Trane and G. J. McLellan, "Relationship between corneal sensitivity, corneal thickness, corneal diameter, and intraocular pressure in normal cats and cats with congenital glaucoma", *Vet. Ophthalmol.* **22** (2019), no. 1, pp. 4–12.

[59] G. Lan, S. R. Aglyamov, K. V. Larin and M. D. Twa, "In vivo human corneal shear-wave optical coherence elastography", *Optom. Vis. Sci.* **98** (2021), no. 1, pp. 58–63.

[60] S. M. Rajaei, F. Asadi, M. R. Rajabian, H. Ostadhassan and M. Crasta, "Effect of body position, eyelid manipulation, and manual jugular compression on intraocular pressure in clinically normal cats", *Vet. Ophthalmol.* **21** (2018), no. 2, pp. 140–143.

[61] E. Ittah, *Hydration-Dependent Structuring in the Cornea: A Model for Bound Water in Collagenous Tissues*, McGill University: Canada, 2023.

[62] Z. Jin, Z. Zhou, M. Shen, Y. Wang, F. Lu and D. Zhu, "Assessment of corneal viscoelasticity using elastic wave optical coherence elastography", *J. Biophotonics* **13** (2020), no. 1, article no. e201960074.

[63] J. R. Crouch, J. C. Merriam and E. R. Crouch III, "Finite element model of cornea deformation", in *International Conference on Medical Image Computing and Computer-Assisted Intervention*, Springer: Berlin, Heidelberg, 2005, pp. 591–598.

[64] A. Elsheikh, "Finite element modeling of corneal biomechanical behavior", *J. Refract. Surg.* **26** (2010), no. 4, pp. 289–300.

[65] G. Pang, C. Wang, X. Wang, X. Li and Q. Meng, "A review of human cornea finite element modeling: geometry modeling, constitutive modeling, and outlooks", *Front. Bioeng. Biotechnol.* **12** (2024), article no. 1455027.

[66] P. Mazinani, C. Cardillo and P. Mosaddegh, "Evaluating corneal biomechanics using shear wave elastography and finite element modeling: sensitivity analysis and parametric optimization", *Continuum. Mech. Thermodyn.* **37** (2025), article no. 12.

[67] A. Nair, Y. S. Ambekar, C. Zevallos-Delgado, et al., "Multiple optical elastography techniques reveal the regulation of corneal stiffness by collagen XII", *Invest. Ophthalmol. Vis. Sci.* **63** (2022), no. 12, article no. 24.

[68] K. C. Shih, R. H. K. Tse, Y. T. Y. Lau and T. C. Y. Chan, "Advances in corneal imaging: current applications and beyond", *Asia-Pac. J. Ophthalmol.* **8** (2019), no. 2, pp. 105–114.

[69] F. Corsi, A. Guandalini, J. L. Rossi Jr, G. Ben-Shlomo, F. Montiani-Ferreira and B. A. Moore, "Ophthalmology of felidae: cats", in *Wild and Exotic Animal Ophthalmology: Volume 2: Mammals*, Springer: Cham, 2022, pp. 155–180.

[70] C. L. De Korte, G. Pasterkamp, A. F. W. van der Steen, H. A. Woutman and N. Bom, "Characterization of plaque components with intravascular ultrasound elastography in human femoral and coronary arteries *in vitro*", *Circulation* **102** (2000), no. 6, pp. 617–623.

[71] A. Elsheikh, D. Alhasso and P. Rama, "Biomechanical properties of human and porcine corneas", *Exp. Eye Res.* **86** (2008), no. 5, pp. 783–790.

[72] C. R. Ethier, M. Johnson and J. Ruberti, "Ocular biomechanics and biotransport", *Annu. Rev. Biomed. Eng.* **6** (2004), pp. 249–273.

[73] P. Su, Y. Yang, J. Xiao and Y. Song, "Corneal hyper-viscoelastic model: Derivations, experiments, and simulations", *Acta Bioeng. Biomech.* **17** (2015), no. 2, pp. 73–84.

[74] M. Friedrich, "Liver fibrosis in viral hepatitis: Noninvasive assessment with acoustic radiation force impulse imaging versus transient elastography", *Radiology* **252** (2009), no. 2, pp. 595–604.

[75] M. R. Bryant and P. J. McDonnell, "Constitutive laws for biomechanical modeling of refractive surgery", *J. Biomech. Eng.* **118** (1996), no. 4, pp. 473–481.

[76] S. D. Carrington and E. G. Woodward, "Corneal thickness and diameter in the domestic cat", *Ophthalmic Physiol. Opt.* **6** (1986), no. 4, pp. 385–389.

[77] P. Su, Y. Yang, J. Xiao and Y. Song, "Corneal hyper-viscoelastic model: derivations, experiments, and simulations", *Acta Bioeng. Biomech.* **17** (2015), no. 2, pp. 73–84.

[78] S. Kling, N. Bekesi, C. Dorronsoro, D. Pascual and S. Marcos, "Corneal viscoelastic properties from finite-element analysis of in vivo air-puff deformation", *PLoS One* **9** (2014), no. 8, article no. e104904.

[79] P.-Y. Chen, C.-C. Shih, W.-C. Lin, T. Ma, Q. Zhou, K. K. Shung and C.-C. Huang, "High-resolution shear wave imaging of the human cornea using a dual-element transducer", *Sensors* **18** (2018), no. 12, article no. 4244.

[80] X. He and J. Liu, "Correlation of corneal acoustic and elastic properties in a canine eye model", *Invest. Ophthalmol. Vis. Sci.* **52** (2011), no. 2, pp. 731–736.

[81] P. Mazinani, H. Setayeshnasab and L. Murcia Terranova, "Evaluating corneal biomechanics using intraocular pressure methods and finite element modeling: parameters study and parametric optimization", *Z. Angew. Math. Phys.* **76** (2025), article no. 220.

[82] P. Mazinani and L. Murcia Terranova, "Finite element simulation for finding shear wave velocity on the canine cornea and sensitivity analysis for IOP parameter", *Mech. Res. Commun.* **150** (2025), article no. 104558.

[83] P. Mazinani and C. Cardillo, "Shear wave velocity and finite element modeling for understanding keratoconus biomechanics: comparison with healthy cornea", *Math. Mech. Solids* (2025).